Commun. Comput. Phys.
doi: 10.4208/cicp.331011.170412s

Vol. **13**, No. 3, pp. 835-850
March 2013

Lattice Boltzmann Study of Flow and Temperature Structures of Non-Isothermal Laminar Impinging Streams

Wenhuan Zhang[1], Zhenhua Chai[2], Zhaoli Guo[1] and Baochang Shi[2,*]

[1] *State Key Laboratory of Coal Combustion, Huazhong University of Science and Technology, Wuhan 430074, China.*
[2] *School of Mathematics and Statistics, Huazhong University of Science and Technology, Wuhan 430074, China.*

Received 31 October 2011; Accepted (in revised version) 17 April 2012

Available online 29 August 2012

Abstract. Previous works on impinging streams mainly focused on the structures of flow field, but paid less attention to the structures of temperature field, which are very important in practical applications. In this paper, the influences of the Reynolds number (Re) and Prandtl number (Pr) on the structures of flow and temperature fields of non-isothermal laminar impinging streams are both studied numerically with the lattice Boltzmann method, and two cases with and without buoyancy effect are considered. Numerical results show that the structures are quite different in these cases. Moreover, in the case with buoyancy effect, some new deflection and periodic structures are found, and their independence on the outlet boundary condition is also verified. These findings may help to understand the flow and temperature structures of non-isothermal impinging streams further.

AMS subject classifications: 76E99

Key words: Impinging streams, lattice Boltzmann method, flow structure, temperature structure.

1 Introduction

Impinging streams (IS) have been used in many industrial applications such as mixing [1,2], absorption [3], liquid-liquid extraction [4] and drying [5], etc. A detailed discussion of IS reactors can be found in [6,7]. Therefore, understanding the flow and temperature structures of such streams is very important for choosing the appropriate operation conditions of processing equipment.

*Corresponding author. *Email addresses:* zwh262308@126.com (W. Zhang), hustczh@126.com (Z. Chai), zlguo@mail.hust.edu.cn (Z. Guo), shibc@mail.hust.edu.cn (B. Shi)

Related studies in the past have shown that the impinging streams are susceptible to instabilities which will lead to asymmetric and deflecting flows. Rolon et al. [10] investigated isothermal impinging streams of air experimentally and observed two different asymmetric stable flows even under the same momentum condition. Denshchikov et al. [8, 9] studied isothermal planar impinging streams of water with experiments and found that each stream was deflected in the opposite direction from the other, and they periodically switched directions.

Motivated by the above findings that show a rich dynamic behavior in impinging streams system, Pawlowski et al. [11] carried out a numerical study of the structure and stability of isothermal laminar impinging streams in planar and cylindrical geometries. For the planar configuration, four flow regimes were found, which are single steady state (symmetric) regime, multiple steady states (asymmetric) regime, deflecting jet regime and vortex shedding regime, respectively. By employing a bifurcation and linearized stability analysis based on the continuity and Navier-Stokes equations, two kinds of bifurcations, i.e., pitchfork bifurcation and Hopf bifurcation, were found. When pitchfork bifurcation and Hopf bifurcation occur, the flow field changes from symmetric regime to asymmetric regime and from asymmetric regime to deflecting jet or vortex shedding regime. Additionally, they also investigated the critical Reynolds number, beyond which the pitchfork or Hopf bifurcation occurs, for different geometry configuration parameters.

In addition to the study of isothermal laminar impinging streams, Hasan et al. [12] performed a numerical investigation of two-dimensional interaction of non-isothermal laminar impinging streams with different fluids (same phase, miscible) in the mixed convection regime. Two kinds of buoyancy, the thermal and the intrinsic buoyancy (owing to the inherently different densities of the two fluids), were considered through the Boussinesq approximation, and two configurations, aiding buoyancy forces and opposing buoyancy forces, were used. For both configurations, some numerical simulations have been conducted under different combinations of Ri_T and Ri_C, which are two important dimensionless numbers in reflecting significance of thermal and intrinsic buoyancy force. The numerical results show that three flow modes, which are symmetric steady flow, asymmetric steady flow and the periodic unsteady flow, may appear depending upon the flow configuration and the effects of the buoyancy forces.

From the survey of available literature, it can be found that above studies were mainly focused on the structures of flow field, but less attention was paid to the structures of temperature field, which are very important in practical applications. To fill this gap, the structures of temperature field with and without buoyancy effect are studied under different Re and Pr, and the relationships between the structures of flow field and the structures of temperature field are also discussed.

In this work, we will study the non-isothermal laminar impinging streams numerically. Among various numerical methods, lattice Boltzmann method (LBM) is a relatively new one and has attracted interest of researchers in a variety of fields [13–15]. Compared to traditional computational fluid dynamics methods, LBM has many advantages, espe-

cially in easy implementation and full parallelism. In addition, since the computational speed on the Graphics processing unit (GPU) is much faster than that on the Central processing unit (CPU), we will use LBM to investigate the non-isothermal laminar impinging streams on GPU [16–18] (we obtain a speedup of one order of magnitude for double precision arithmetic with respect to the computational performance of CPU).

The rest of paper is organized as follows. The problem description is given in Section 2. The lattice Boltzmann method is introduced in Section 3. In Section 4, numerical results and discussion are given. And finally conclusions are presented in Section 5.

2 Problem description

The configuration of impinging streams is illustrated in Fig. 1, which is used in the present study since it is a benchmark one [11, 12]. The basic phenomenon of such problem is that two identical jets with uniform velocity U are ejected from inlet1 and inlet2 and then collide with each other. After the jets change their flow direction, they begin to flow out. As shown in Fig. 1, W is the width of the inlet, H is the separation between two jets, L is the total length of the channel.

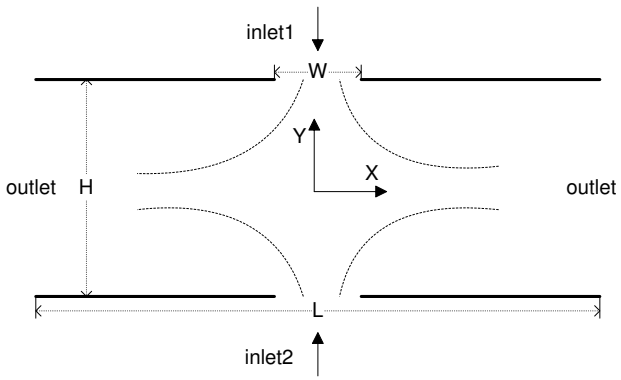

Figure 1: Configuration of impinging streams.

Based on the assumptions that the flow is laminar and the fluid is incompressible and Newtonian, the dimensionless governing equations can be written as follows:

$$\nabla\cdot\mathbf{u}=0, \tag{2.1a}$$

$$\frac{\partial\mathbf{u}}{\partial t}+\mathbf{u}\cdot\nabla\mathbf{u}=-\nabla p+\frac{1}{Re}\nabla^2\mathbf{u}+Ri\Theta\mathbf{k}, \tag{2.1b}$$

$$\frac{\partial\Theta}{\partial t}+\mathbf{u}\cdot\nabla\Theta=\frac{1}{Re\cdot Pr}\nabla^2\Theta, \tag{2.1c}$$

where $\nabla=\left(\partial/\partial x,\partial/\partial y\right)$, x,y are the dimensionless space coordinates, t is the dimensionless time coordinate. $\mathbf{u}=(u,v)$, p and Θ are the dimensionless velocities, pressure and

temperature, respectively. **k** is the unit vector in the y direction. The dimensionless temperature is defined as $\Theta=(T-T_0)/\Delta T$, where $T_0=(T_1+T_2)/2$, $\Delta T=(T_2-T_1)$ $(T_2>T_1)$, T_1 and T_2 are the temperature of jets ejected form inlet1 and inlet2, respectively. The dimensionless numbers in Eq. (2.1) are defined as, $Re=WU/\nu$, $Pr=\nu/D$ and $Ri=|\mathbf{g}|\beta\Delta TW/U^2$, where ν, D, β and **g** are the kinematic viscosity, coefficient of thermal diffusion, coefficient of thermal expansion and acceleration vector of gravity.

The boundary conditions of present problem are set as follows (see Fig. 1 for the meaning of symbols used):

inlet1:

$$\left(y=\frac{H}{2};-\frac{W}{2}<x<\frac{W}{2}\right) \qquad u=0, \quad v=-1, \quad \Theta=-0.5, \tag{2.2}$$

inlet2:

$$\left(y=-\frac{H}{2};-\frac{W}{2}<x<\frac{W}{2}\right) \qquad u=0, \quad v=1, \quad \Theta=0.5, \tag{2.3}$$

top and bottom walls:

$$\left(y=\pm\frac{H}{2};x>\frac{W}{2}\ or\ x<-\frac{W}{2}\right) \qquad u=v=0, \quad \frac{\partial\Theta}{\partial y}=0, \tag{2.4}$$

outlet:

$$\left(x=\pm\frac{L}{2};-\frac{H}{2}<y<\frac{H}{2}\right) \qquad \frac{\partial u}{\partial x}=\frac{\partial v}{\partial x}=\frac{\partial\Theta}{\partial x}=0. \tag{2.5}$$

The initial values of u,v,p and Θ were set to be zero everywhere except two jet inlets. To reduce the effects of exit boundary condition on the structures of flow and temperature fields, we set L/H to be 20. In addition, the value of configuration parameter α (H/W) is fixed to be 4.

3 Numerical method

Instead of solving the continuum hydrodynamics equation, LBM deals with the evolution of discrete single-particle velocity distribution functions in time and space. In an early work, a lattice Boltzmann formulation for the Boussinesq equations with a separate scalar temperature field has been introduced by He et al. [19], in combination with the modification given in [20] that eliminates the compressibility error in the steady state. After that, some simpler models are also proposed by Guo and Shi et al. [21–23]. In the present work, the thermal lattice model presented in [21] (TD2G9 model) is used.

In the TD2G9 model, the evolution equations for velocity and temperature fields are as follows:

$$g_i(\mathbf{x}+c\mathbf{e}_i\Delta t,t+\Delta t)-g_i(\mathbf{x},t)=-\frac{1}{\tau_{\mathbf{u}}}(g_i(\mathbf{x},t)-g_i^{(eq)}(\mathbf{x},t))+f_i(\mathbf{x},t), \quad i=0-8, \tag{3.1a}$$

$$\Theta_i(\mathbf{x}+c\mathbf{e}_i\Delta t,t+\Delta t)-\Theta_i(\mathbf{x},t)=-\frac{1}{\tau_\Theta}(\Theta_i(\mathbf{x},t)-\Theta_i^{(eq)}(\mathbf{x},t)), \qquad i=1-4, \tag{3.1b}$$

where $\mathbf{e}_i$ is the discrete velocity direction, $c=\triangle x/\triangle t$ is the particle speed ($c=10$ is set in our simulations), $\triangle x$ and $\triangle t$ are the lattice spacing and the time increment, respectively. $\tau_{\mathbf{u}}$ and τ_Θ characterize the relaxation times of distribution functions $g_i(\mathbf{x},t)$ and $\Theta_i(\mathbf{x},t)$ towards the local equilibriums $g_i^{(eq)}(\mathbf{x},t)$ and $\Theta_i^{(eq)}(\mathbf{x},t)$. $f_i(\mathbf{x},t)$ is defined by $f_i(\mathbf{x},t)=\Delta t\alpha_i\mathbf{e}_i\cdot\mathbf{k}Ri\Theta/(2c)$, where $\alpha_i=\delta_{i2}+\delta_{i4}$.

The velocity directions $\mathbf{e}_i$ for TD2G9 model are given by

$$\mathbf{e}_i=\begin{cases}(0,0), & i=0,\\ \Big(\cos\dfrac{(i-1)\pi}{2},\sin\dfrac{(i-1)\pi}{2}\Big), & i=1,2,3,4,\\ \sqrt{2}\Big(\cos\Big[\dfrac{(i-5)\pi}{2}+\dfrac{\pi}{4}\Big],\sin\Big[\dfrac{(i-5)\pi}{2}+\dfrac{\pi}{4}\Big]\Big), & i=5,6,7,8.\end{cases}\tag{3.2}$$

The equilibrium distribution function $g_i^{(eq)}(\mathbf{x},t)$ is defined by

$$g_i^{(eq)}(\mathbf{x},t)=\begin{cases}-4\sigma\dfrac{p}{c^2}+s_i(\mathbf{u}), & i=0,\\ \lambda\dfrac{p}{c^2}+s_i(\mathbf{u}), & i=1,2,3,4,\\ \gamma\dfrac{p}{c^2}+s_i(\mathbf{u}), & i=5,6,7,8,\end{cases}\tag{3.3}$$

where σ, λ and γ are parameters satisfying $\lambda+\gamma=\sigma$, $\lambda+2\gamma=1/2$, $s_i(\mathbf{u})=\omega_i[3\mathbf{e}_i\cdot\mathbf{u}/c+4.5(\mathbf{e}_i\cdot\mathbf{u})^2/c^2-1.5|\mathbf{u}|^2/c^2]$, $\omega_0=4/9$, $\omega_i=1/9\,(i=1-4)$ and $\omega_i=1/36\,(i=5-8)$. In the simulation, $\sigma=5/12$, $\lambda=1/3$ and $\gamma=1/12$ are set such that $\lambda:\gamma=\omega_1:\omega_5$.

The equilibrium distribution function $\Theta_i^{(eq)}(\mathbf{x},t)$ is defined by

$$\Theta_i^{(eq)}(\mathbf{x},t)=\frac{\Theta}{4}\Big[1+2\frac{\mathbf{e}_i\cdot\mathbf{u}}{c}\Big],\quad i=1,2,3,4.\tag{3.4}$$

The fluid velocity, pressure and temperature can be calculated as

$$\mathbf{u}=\sum_i c\mathbf{e}_i g_i,\quad p=\frac{c^2}{4\sigma}\Big[\sum_{i\neq0}g_i+s_0(\mathbf{u})\Big],\quad \Theta=\sum_i\Theta_i.\tag{3.5}$$

The transport coefficients are determined by

$$\nu=\frac{1}{3}\Big(\tau_{\mathbf{u}}-\frac{1}{2}\Big)\frac{\Delta x^2}{\Delta t},\quad D=\frac{1}{2}\Big(\tau_\Theta-\frac{1}{2}\Big)\frac{\Delta x^2}{\Delta t}.\tag{3.6}$$

Through the Chapman-Enskog expansion, the governing equations (2.1) can be recovered. The non-equilibrium extrapolation scheme [24, 25] is used to calculate the distribution functions at the boundaries and its principle is as follows. Firstly, the distribution functions $m_i(x,t)$ (=$g_i(x,t)$ or $\Theta_i(x,t)$) at the boundaries can be decomposed into two parts, that is, $m_i(B,t)=m_i^{(eq)}(B,t)+m_i^{(neq)}(B,t)$, where B denotes the boundary point,

$m_i^{(neq)}(B,t)$ is the non-equilibrium part of distribution function. Secondly, we approximate the non-equilibrium part of distribution function at the boundary point with that at the neighbouring fluid node, i.e., $m_i^{(neq)}(B,t) \approx m_i^{(neq)}(I,t) = m_i(I,t) - m_i^{(eq)}(I,t)$, where I is the neighbouring fluid point. Generally, $m_i^{(eq)}(B,t)$ is calculated with the macroscopic velocities and temperature at the boundaries which are determined by Eqs. (2.2)-(2.5). For $m_i(I,t)$ and $m_i^{(eq)}(I,t)$, they are already known before dealing with the distribution functions at the boundaries.

4 Numerical results and discussion

4.1 Validation

Before we proceed any further, the validation of numerical method is first conducted by comparing the velocity and Nusselt number distributions with the previous results [12, 26]. To present the comparison, the symmetric condition was imposed at the centerline $x=0$, the temperatures of walls were kept at zero and the temperatures of jets were kept at 0.5. The computations were carried out with the grid size of 81×1601, and this grid size was found to be adequate for giving grid-independent results. In Fig. 2(a), where $\alpha=2$ and $Re=100$, the velocity profile at the location of $x/H=4$ is presented, and compared with some previous results, y has been normalized with H, U (horizontal velocity) has been normalized with the average velocity U_{ave} at $x/H=4$. In Fig. 2(b), where $\alpha=4$ and $Re=250$, we present the Nusselt number (Nu) profile along the top wall, and compare it with some available results. It should be noted that the flow field for this case is a mirror image of that obtained in previous works, which is attributed to the pitchfork bifurcation of fluid flow. The Nusselt number is based on the bulk temperature and has been normalized by the corresponding value of the fully developed plane Poiseuille flow. As seen from Fig. 2, the velocity and Nusselt number distributions are in good agreement with the results obtained from [12, 26].

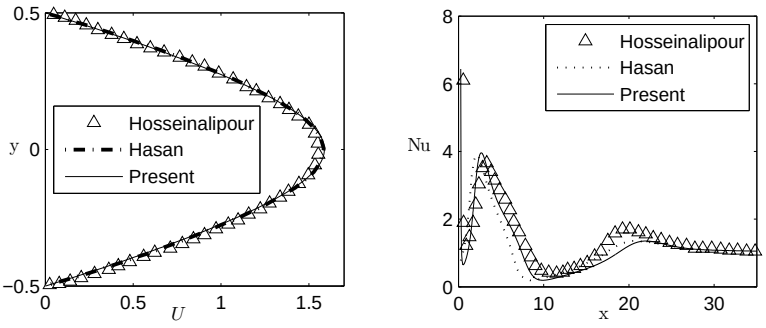

(a) velocity distribution (b) Nusselt number distribution

Figure 2: The comparison of velocity and Nusselt number distributions with the previous works.

4.2 The case without buoyancy effect

In this subsection, the buoyancy effect is not considered, i.e., $Ri=0$.

We first study the influences of Re on the structures of flow and temperature fields, and show the results in Fig. 3. As seen from this figure, the flow fields are symmetric at $Re=30$ and $Re=45$, but asymmetric for $Re=75$ and $Re=90$, this is because the increase of Re leads to the occurring of pitchfork bifurcation. In addition, the structures of temperature field are similar to those of flow field, as shown in Fig. 3, for $Re=30$ and $Re=45$, the temperature fields are symmetric about the midplane, the lower(<0) and higher(>0) temperatures are distributed above and below the midplane, respectively. When Re is increased to 75, the temperature field becomes asymmetric, the lower and higher temperatures have crossed the midplane and entered the domain below and above it. When Re is further increased to 90, the temperature field is still asymmetric. The structure similarity between both fields can be attributed to the fact that the temperature field is mainly affected by the flow field.

The influences of Pr on the structures of flow and temperature fields are also studied, and shown in Fig. 4. As seen in this figure, the temperature is mainly distributed along the centerline in y direction for $Pr=0.1$. As Pr increases to 0.5, the temperature distribution extends to a larger region. When Pr is further increased to 1.0 or 2.0, the temperature is distributed in the entire domain. Therefore, it can be concluded that the temperature distribution is more and more uniform as Pr increases. This is because the thermal advection is more and more significant compared to the thermal diffusion with the increase of Pe, which is defined as $Re\cdot Pr$. Although the uniformity of temperature distribution is affected by Pr, the symmetric structure of temperature field is not changed for different Pr, see Fig. 4. Additionally, the structure of flow field keeps unchanged for different Pr since the flow field is not affected by the temperature field.

4.3 The case with buoyancy effect

In this part, we present a detailed parameter study on the case with buoyancy effect, and pay attention to the buoyancy effect on the structures of flow and temperature fields.

Firstly, the influences of Ri on the structures of flow and temperature fields are studied, and shown in Fig. 5. From this figure, it can be found that the flow and temperature fields are both symmetric about the midplane at $Ri=0.1$, and such symmetry is similar to the case at $Ri=0$, which implies the buoyancy force has no apparent effect on the structures of flow and temperature fields under such small Ri. However, when Ri is increased to 0.45, the flow and temperature fields become asymmetric, which is attributed to the fact that large buoyancy force accelerates the fluid ejected from jet inlets, and finally causes the occurring of pitchfork bifurcation. As Ri increases to 0.7, the jets deflect off each other in the opposite direction and flow out of the channel from the left and right outlets. Because the jets have different temperatures, the higher and lower temperatures are distributed in the regions through which the hotter and colder jets have flowed out.

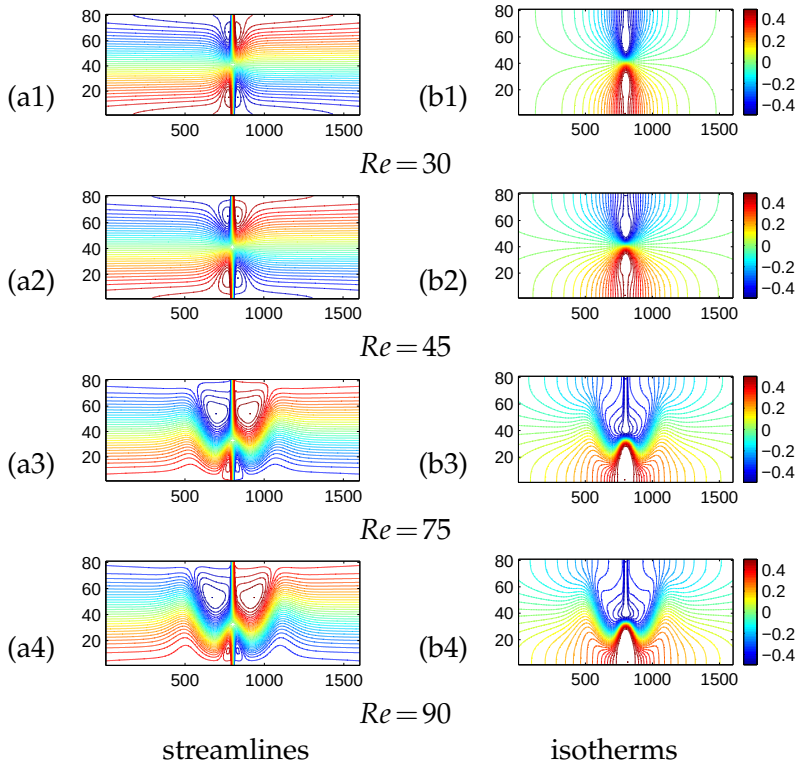

Figure 3: Streamlines and isotherms of impinging streams for different Re, $\alpha=4$, $Pr=1.0$, $Ri=0$.

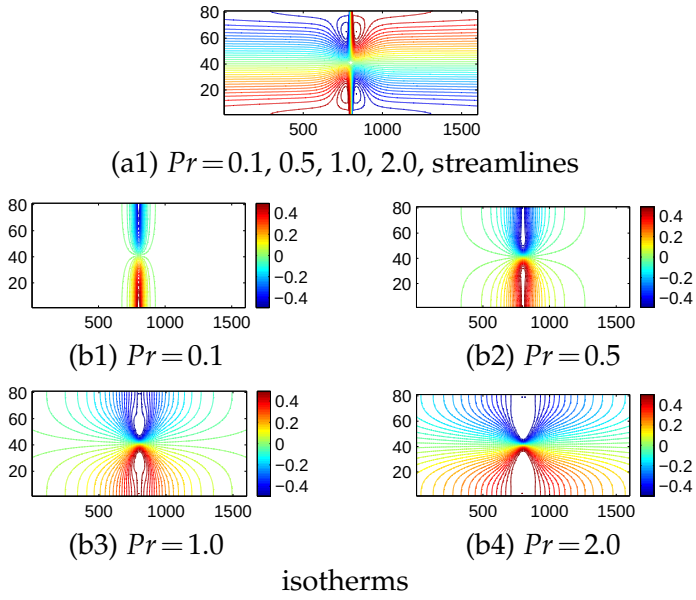

Figure 4: Streamlines and isotherms of impinging streams for different Pr, $\alpha=4$, $Re=45$, $Ri=0$.

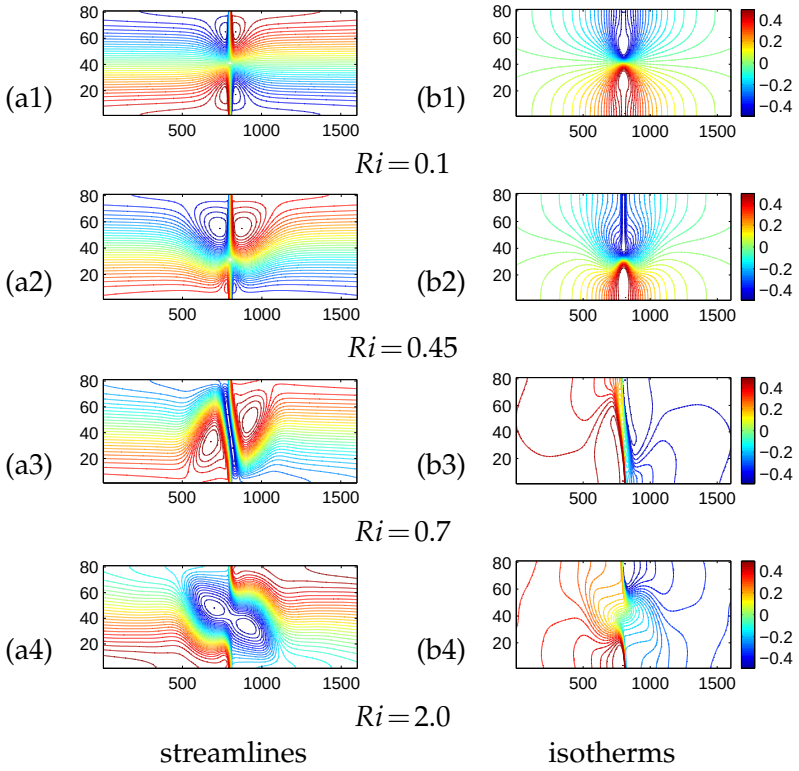

Figure 5: Streamlines and isotherms of impinging streams for different Ri, $\alpha=4$, $Re=45$, $Pr=1.0$.

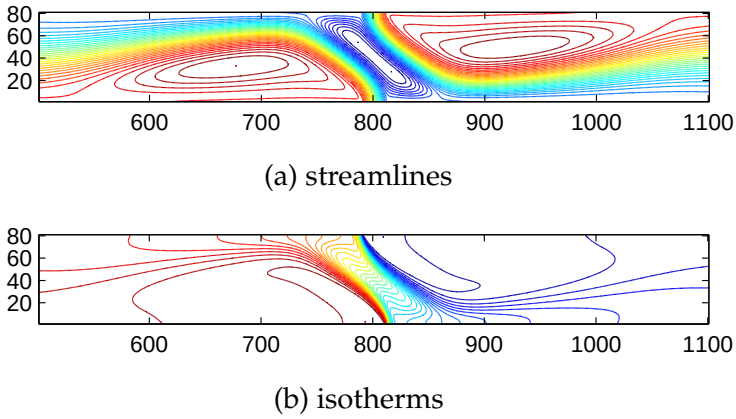

Figure 6: Close-up views of flow and temperature fields of impinging streams for Ri=0.7, α=4, Re=45, Pr=1.0.

In fact, there are three vortices in the flow field at $Ri=0.7$, as seen in Fig. 6. The vortex in the center region is induced probably by the combination effects of "natural convection" between two jets with different temperatures and the opposite velocities of two jets. In

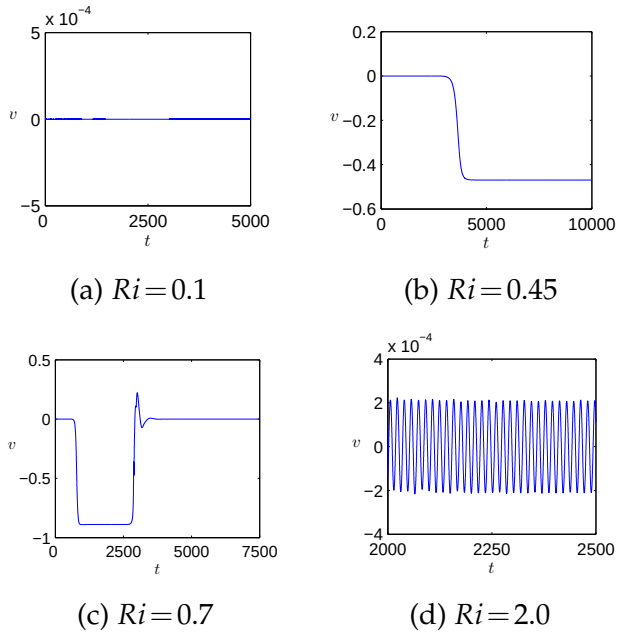

(a) $Ri=0.1$ (b) $Ri=0.45$

(c) $Ri=0.7$ (d) $Ri=2.0$

Figure 7: The dimensionless time history of v(0,0) of impinging streams for different Ri, $\alpha=4$, $Re=45$, $Pr=1.0$.

addition, the isotherms in the center region are nearly horizontal, which means that the heat transfer mechanism is dominated by convection. When Ri is further increased to 2.0, the vortex in the center region breaks up into two vortices, and the isotherms in the center region become more horizontal. The changes of streamlines and isotherms from $Ri=0.7$ to $Ri=2.0$ are very similar to those of natural convection flow in a square cavity with the increase of Rayleigh number [27,28].

We also present the dimensionless time history profiles of v at origin of coordinates for different Ri in Fig. 7. As seen from this figure, v is always zero for Ri=0.1, at which the flow field is symmetric. For the case of $Ri=0.45$, v changes from zero to a constant, and correspondingly, the flow field changes from symmetric structure to asymmetric structure. When $Ri=0.7$, after v keeps unchanged at a constant, its value returns to zero, but the flow field changes into the deflection structure. When Ri increases to 2.0, the profile shows that the flow becomes periodic (streamlines and isotherms in Fig. 5 (a4) and (b4) represent the structures of mean velocity and temperature distributions). From above observations, it can be found that the increase of Ri makes the flow more and more unstable, and thus, the state of v changes more and more frequently. In addition, similar profiles of temperature at the origin of coordinates are also observed.

Secondly, the influences of Re on the structures of flow and temperature fields for the case of $Ri=0.45$ are investigated, and shown in Fig. 8. As seen from this figure, when the buoyancy effect ($Ri=0.45$) is included, the flow and temperature fields are still symmetric at $Re=30$, but asymmetric at $Re=45$. When Re is increased to 75, the

deflection structures of flow and temperature fields are observed and these structures are similar to those in Fig. 5 (a3) and (b3), but with opposite deflection direction. As Re increases to 90, an unsteady periodic flow is observed, and the distribution of mean velocity presents the asymmetric structure, in which two much larger recirculation zones appear near the upper jet inlet, compared with the structure in Fig. 8 (a2). From above discussions, it can be deduced that, compared with the case without buoyancy effect, the flow and temperature fields with buoyancy effect present more structures.

Thirdly, the influences of Pr on the structures of flow and temperature fields are also studied, and shown in Fig. 9. From this figure, it can be seen that the uniformity of temperature distribution is enhanced as Pr increases. This is because the increase of Pr makes the heat convection more and more significant than the heat conduction. In addition, it can also be seen that the structure of temperature field changes with the increase of Pr. For the cases of $Pr=0.1$ and $Pr=1.0$, the temperature fields are asymmetric about the midplane. Because of the complex interactions between flow and temperature fields, the temperature field presents the deflection structure for the case of $Pr=0.5$. When Pr is increased to 2.0, the periodic structure of temperature field was observed (isotherms shown in Fig. 9 (b4) represent the structure of mean temperature distribution). Thus, it can be concluded that the increase of Pr for the case with buoyancy effect not only enhances the uniformity of temperature distribution but also changes the structure of temperature field. Additionally, because the flow field is affected by the buoyancy effect, the increase of Pr leads to the changes of flow filed, which are similar to those of the temperature field. Finally, it is worth mentioning that two interesting phenomena are observed in Fig. 9 (b4). Firstly, the distributions of higher and lower temperatures in the center region seem to be confined in two rectangular boxes. Secondly, outside of the boxes, the colder temperature is distributed below the midplane and the higher temperature is distributed above the midplane. The explanation of the latter phenomenon can be found from the instantaneous temperature field shown in Fig. 10. From this figure, it can be seen that the vortices in the temperature field make the higher temperature enter the domain above the midplane and the lower temperature enter the domain below the midplane.

Based on the results presented above, it can be concluded that there are four types of flow and temperature structures under different Ri, Re and Pr, which are symmetric structure, asymmetric structure, deflection structure and periodic structure. For the deflection structure, the periodic reversals of the deflection direction reported in the previous works [8,9,11] are not observed here, which may be due to the buoyancy effect. To check whether the lack of reversals is due to a finite Mach number effect, we have run the code with a larger c, say c=15 or 20, and found that the deflection direction is still not reversed. For this reason, we can conclude that the lack of reversals is not caused by the variation of Mach number. Additionally, for periodic structures shown in Fig. 5, Fig. 8 and Fig. 9, we present the instantaneous flow fields in Fig. 11. As shown in Fig. 11 (b) and (c), some vortices are formed near the channel walls, this phenomenon has been reported by Hasan et al. [12] for the first time, but two recirculation zones at each side of y axis are the same with each other in their work, which is different from present results.

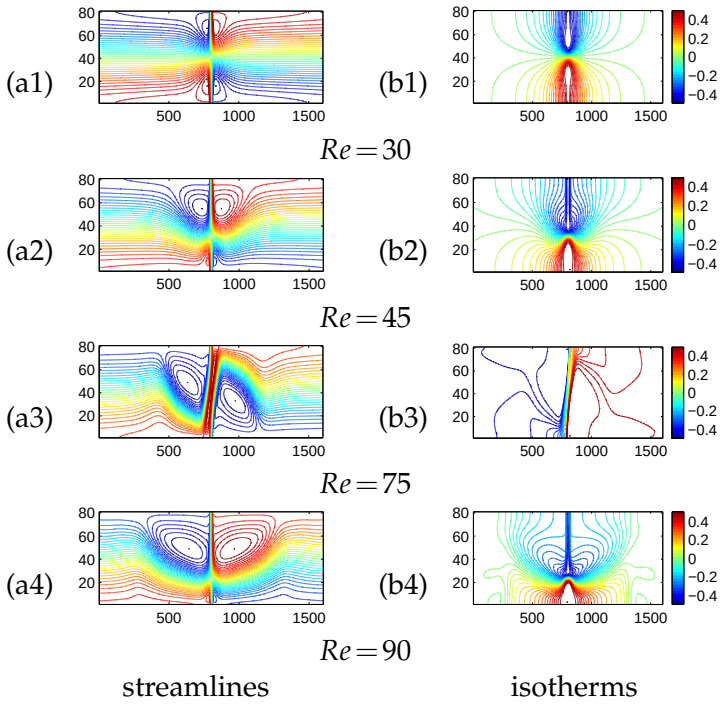

Figure 8: Streamlines and isotherms of impinging streams for different Re, $\alpha=4$, $Pr=1.0$, $Ri=0.45$.

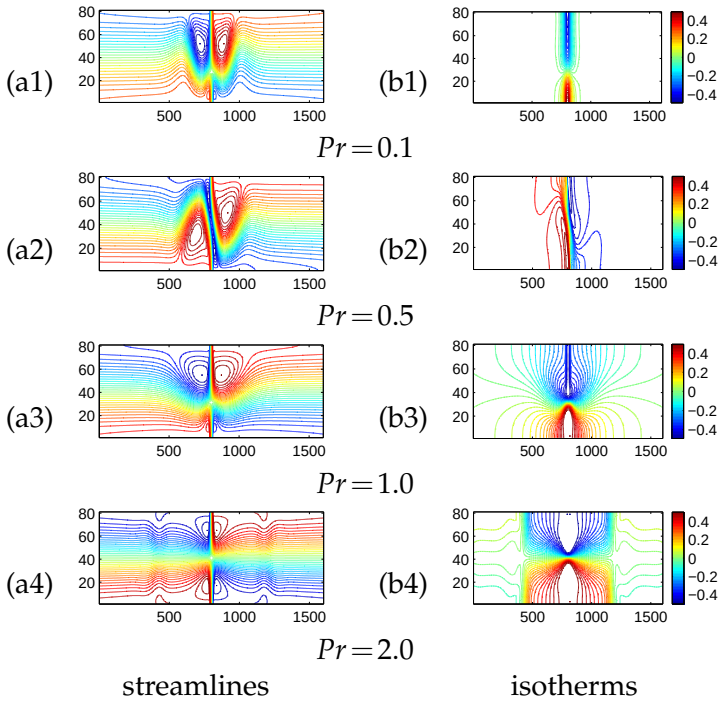

Figure 9: Streamlines and isotherms of impinging streams for different Pr, $\alpha=4$, $Re=45$, $Ri=0.45$.

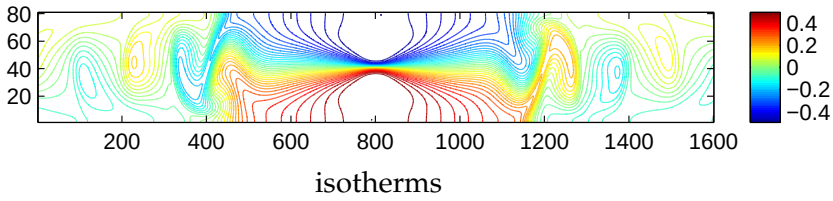

isotherms

Figure 10: Instantaneous temperature field of impinging streams for $\alpha=4, Ri=0.45,\ Re=45,\ Pr=2.0$.

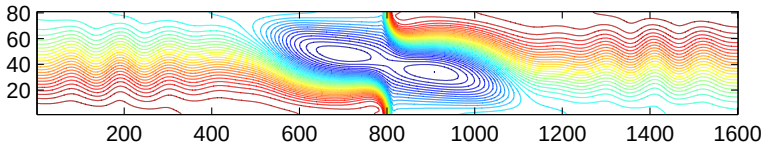

(a) $Ri=2.0,\ Re=45,\ Pr=1.0$

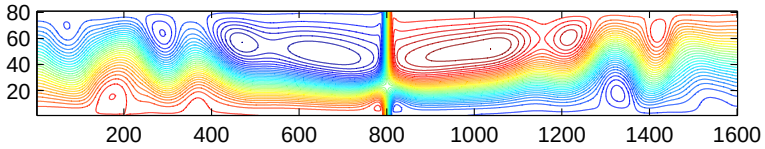

(b) $Ri=0.45,\ Re=90,\ Pr=1.0$

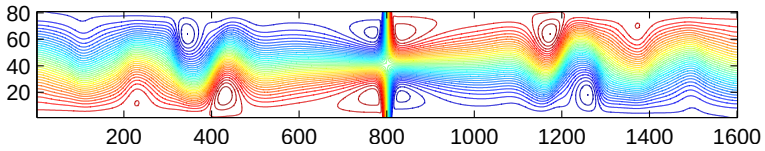

(c) $Ri=0.45,\ Re=45,\ Pr=2.0$

streamlines

Figure 11: Instantaneous flow fields of impinging streams for different cases, $\alpha=4$.

4.4 The boundary condition effects on the new structures

The outlet boundary condition $\partial u/\partial x=\partial v/\partial x=\partial\Theta/\partial x=0$ (in Eq. (2.5)) is based on the assumption of fully developed flow and has been used in many works on the impinging streams [29, 30]. But different velocity and temperature boundary conditions which are $\partial u/\partial x=0, v=0$ and $\partial^2\Theta/\partial x^2=0$ were also used, such as in [11] and [12], respectively. Because we found the deflection structure for the first time and some new periodic structures, it is necessary to verify if these structures are affected by the choices of these different outlet boundary conditions. Two typical cases which are $Ri=0.7, Re=45, Pr=1.0$ (deflection structure, case 1) and $Ri=0.45, Re=45, Pr=2.0$ (periodic structure, case 2) were used to examine the effects of $\partial u/\partial x=0, v=0$ and $\partial^2\Theta/\partial x^2=0$ on the new structures.

We first carried out the simulation with the input parameters of case 1 under the condition of $\partial u/\partial x=0, v=0, \partial\Theta/\partial x=0$, it is found that the steady flow field still present the

deflection structure, and the global relative differences of u and v under this condition and that in Eq. (2.5) are 0.039% and 0.17%, which means $\partial u/\partial x=0$, $v=0$ doesn't affect the structure of flow field. We secondly implemented the simulation with the input parameters of case 2 under the condition $\partial u/\partial x=0$,$\partial v/\partial x=0$,$\partial^2\Theta/\partial x^2=0$, it is found that the structure of instantaneous temperature field is nearly the same with that under the condition in Eq. (2.5), and the global relative difference of mean temperature is 1.18%, which means $\partial^2\Theta/\partial x^2=0$ doesn't affect the structure of temperature field. In addition, we double the channel length to validate the periodic structure in case 2, it is found that the structure of instantaneous temperature field in the central part of enlarged domain is still unchanged.

5 Conclusions

In this paper, the study of flow and temperature structures of non-isothermal laminar impinging streams is performed with the lattice Boltzmann method, two cases with and without buoyancy effect are considered.

For the case without buoyancy effect, it is found that the flow and temperature fields change from symmetric structure to asymmetric structure with the increase of Re. When Pr is increased, the temperature distribution is more and more uniform in the entire domain but the structure of flow field is not changed, which is because the flow field is not affected by the temperature field.

For the case with buoyancy effect, it is found that the flow and temperature fields become more and more unstable with the increase of Ri. When Re is increased, the flow and temperature fields present more structures than those of the case without buoyancy effect. In addition, as the Pr increases, the uniformity of temperature distribution is enhanced and the structures of flow and temperature fields are changed. According to the results of this case, four types of flow and temperature structures are found, which are symmetric structure, asymmetric structure, deflection structure and periodic structure, and what is more, the steady deflection structure presented in our work has not been reported in available works, some different periodic structures are also observed.

Finally, the present work provides rich information about the flow and temperature structures of non-isothermal impinging streams, which may be used as a reference to understand the structures of impinging streams further.

Acknowledgments

The work is supported by National Natural Science Foundation of China (Grant Nos. 51006040, 51006039) and the Fundamental Research Funds for the Central Universities, HUST (Grant Nos. 2010JC005, 2010MS131 and 2010QN057).

References

[1] P. Wood, A. Hrymak, R. Yeo, D. Johnson and A. Tyagi, Experimental and computational studies of the fluid mechanics in an opposed jet mixing head, Phys. Fluids A, 3 (1991), 1362-1368.

[2] R. J. Santos, A. M. Teixeira, and J. B. Lopes, Study of mixing and chemical reaction in RIM, Chem. Eng. Sci., 60 (2005), 2381-2398.

[3] Y. Bermana, A. Tanklevskya, Y. Orenb and A. Tamira, Modeling and experimental studies of SO2 absorption in coaxial cylinders with impinging streams: part II, Chem. Eng. Sci., 55 (2000), 1023-1028.

[4] A. M. Dehkordi, Application of a novel-opposed-jets contacting device in liquid-liquid extraction, Chem. Eng. Process., 41 (2002), 251-258.

[5] S. M. Hosseinalipour and A. S. Mujumdar, Flow, Heat Transfer and Particle Drying Characteristics in Confined Opposing Turbulent Jets: a Numerical Study, Drying Technol., 13 (1995), 753-781.

[6] A. Tamir, Impinging-stream reactors: fundamentals and applications, Elsevier, 1994.

[7] Y. Wu, Impinging streams: fundamentals, properties and applications, Elsevier, 2007.

[8] V. A. Denshchikov, V. N. Kontratev and A. N. Romashev, Interaction between two opposed jets, Fluid Dyn., 13 (1978), 924-926.

[9] V. A. Denshchikov, V. N. Kontratev, A. N. Romashev and V. M. Chubarov, Auto-oscillations of planar colliding jets, Fluid Dyn., 18 (1983), 460-462.

[10] J. C. Rolon, D. Veynante and J. P. Martin, Counter jet stagnation flows, Exp. Fluids, 11 (1991), 313-324.

[11] R. P. Pawlowski, A. G. Salinger, J. N. Shadid and T. J. Mountziaris, Bifurcation and stability analysis of laminar isothermal counterflowing jets, J. Fluid Mech., 551 (2006), 117-139.

[12] N. Hasan and S. A. Khan, Two-dimensional interactions of non-isothermal counter-flowing streams in an adiabatic channel with aiding and opposing buoyancy, Int. J. Heat Mass Transfer, 54 (2011), 1150-1167.

[13] Y. H. Qian, S. Succi and S. A. Orszag, Recent advances in Lattice Boltzmann computing, Annu. Rev. Comput. Phys., 3 (1995), 195-242.

[14] S. Y. Chen and G. D. Doolen, Lattice Boltzmann method for fluid flows, Annu. Rev. Fluid Mech., 30 (1998), 329-364.

[15] C. K. Aidun and J. R. Clausen, Lattice-Boltzmann Method for Complex Flows, Annu. Rev. Fluid Mech., 42 (2010), 439-472

[16] J. T*ö*lke, Implementation of a Lattice Boltzmann kernel using the Compute Unified Device Architecture developed by nVIDIA, Comput. Visualization Sci., 13 (2008), 29-39.

[17] J. Tölke and M. Krafczyk, TeraFLOP computing on a desktop PC with GPUs for 3D CFD, Int. J. Comput. Fluid Dyn., 22 (2008), 443-456.

[18] M. Bernaschi, L. Rossi, R. Benzi, M. Sbragaglia and S. Succi, Graphics processing unit implementation of lattice Boltzmann models for flowing soft systems, Phys. Rev. E, 80 (2009), 066707.

[19] X. Y. He, S. Y. Chen and G. D. Doolen, A novel thermal model of the lattice Boltzmann method in incompressible limit, J. Comput. Phys., 146 (1998), 282-300.

[20] X.Y. He and L.S. Luo, Lattice Boltzmann Model for the Incompressible Navier-Stokes Equation, J. Stat. Phys., 88 (1997), 927-944.

[21] Z. L. Guo, B. C. Shi and C. G. Zheng, A coupled lattice BGK model for the Boussinesq equations, Int. J. Numer. Methods Fluids, 39 (2002), 325-342.

[22] Z. L. Guo, B. C. Shi and N. C. Wang, Lattice BGK Model for Incompressible Navier-Stokes Equation, J. Comput. Phys., 165 (2000), 288-306.
[23] B. C. Shi, N. Z. He and N. C. Wang, A unified thermal Lattice BGK model for Boussinesq equations, Prog. Comput. Fluid Dyn., 5 (2005), 50-64.
[24] Z. L. Guo, C. G. Zheng and B. C. Shi, Non-equilibrium extrapolation method for velocity and pressure boundary conditions in the lattice Boltzmann method, Chin. Phys., 11 (2002), 366-374.
[25] Z. L. Guo, C. G. Zheng and B. C. Shi, An extrapolation method for boundary conditions in lattice Boltzmann method, Phys. Fluids, 14 (2002), 2007-2010.
[26] S. M. Hosseinalipour and A. S. Mujumdar, Flow and thermal characteristics of steady two-dimensional confined laminar opposing jets: Part I. Equal Jets, Int. Commun. Heat Mass Transfer, 24 (1997), 27-38.
[27] M. Hortmann, M. Perić and G. Scheuerer, Finite volume multigrid prediction of laminar natural convection: bench-mark solutions, Int. J. Numer. Methods Fluids, 11 (1990), 189-207.
[28] G. Barakos, E. Mitsoulis and D. Assimacopoulos, Natural convection flow in a square cavity revisited: laminar and turbulent models with wall functions, Int. J. Numer. Methods Fluids, 18 (1994), 695-719.
[29] S. Devahastin and A. S. Mujumdar, A numerical study of flow and mixing characteristics of laminar confined impinging streams, Chem. Eng. J., 85 (2002), 215-223.
[30] S. Devahastin and A. S. Mujumdar, A numerical study of mixing in a novel impinging stream in-line mixer, Chem. Eng. Process., 40 (2001), 459-470.